Time-Resolved Raman-Scattering with Incoherent-Light

Wynne, K.; Muller, M.; Vanvoorst, J.D.W.

DOI
10.1103/PhysRevA.41.6361
Publication date
1990

Published in
Physical Review A

Time-resolved Raman scattering with incoherent light

Klaas Wynne, M. Müller, and J. D. W. Van Voorst
Laboratory for Physical Chemistry, University of Amsterdam, Nieuwe Achtergracht 127, 1018 WS Amsterdam, The Netherlands
(Received 28 November 1989)

In time-resolved Raman scattering (as well as in degenerate four-wave mixing) the time resolution is in principle determined by the coherence time of the laser pulses involved rather than the pulse widths. In this paper the theoretical time dependence of three different time-resolved Raman-scattering techniques, Raman-fringe decay (RFD), coherent Stokes Raman scattering, and time-resolved stimulated Raman gain, is calculated under various coherence conditions of the fields. Taking RFD generated by temporally incoherent light as the example, it is shown that due to complicated coherence effects the material relaxation time cannot be extracted from the experimental data without careful consideration of the stochastic properties of the fields and the different relaxation parameters of the system. The RFD technique has been experimentally applied to the 524-cm^{-1} mode of CH_3I and the 656-cm^{-1} mode of CS_2 and coherence effects are indeed observed. The relaxation times are found to be in agreement with previous experimental studies with coherent light.

I. INTRODUCTION

Investigations in the time domain are often preferred in favor of spectral studies, because the relaxation phenomena may be studied directly without an intervening Fourier transform. It is, however, unfortunate that many of the interesting relaxation phenomena in the liquid and solid state take place on a subpicosecond or femtosecond time scale. Although the knowledge of the generation of ultrashort optical pulses has increased rapidly in the last decade, the practical application is still difficult due to the limited frequency tunability of the available femtosecond dye lasers and pulse-broadening effects in the experimental setup.[1] A few years ago it was noted that under special circumstances the time resolution in optical experiments is not so much determined by the width of the electromagnetic pulses but by the coherence time of the (partially coherent) fields involved. Although dispersive elements in a setup may still affect the theoretical time resolution to be achieved with broadband incoherent light, at least the restrictions on tunability are much less severe.

The theoretical prediction that greater time resolution can be achieved with broadband incoherent light in degenerate four-wave mixing (DFWM) was made by Morita and Yajima[2-4] and was subsequently verified by several experiments, i.e., in pump and probe,[5,6] photon echo,[7-12] (heterodyne-detected) accumulated photon echo,[13-16] Kerr effect,[17-20] and others.[21] A similar effect can also be observed in coherent Stokes Raman scattering[18,19,22] (CSRS) if the two Stokes pulses (for excitation and probing, see below) are temporally incoherent and mutually correlated. The slight disadvantage of incoherent CSRS is that the signal has a large background and a coherence spike at zero delay. Other authors (e.g., Refs. 23 and 24) suggested that if the probe pulse in CSRS is replaced by a probe-pulse pair consisting of laser and Stokes pulses, greater time resolution can also be achieved but without or nearly without a background or spike. The effect of adding an extra pulse to the probe pulse in CSRS is that various combinations of pulses induce interfering signal fields. The oscillating part of the total signal is easily extracted and is of interest for the study of relaxation phenomena. If the signal is detected at the Stokes frequency (that is, at the frequency of one of the probe fields) the result is called time-resolved stimulated Raman gain (TSRG). Due to the frequency degeneracy the generated Stokes field can only be heterodyne-detected with the corresponding higher signal intensities. If the signal is detected at the anti-Stokes frequency, the Raman-fringe decay (RFD) results; this is very similar to TSRG. To assess the performance of the respective techniques, the three types of time-resolved Raman scattering will be described in a unified framework.

Section II is devoted to the theoretical description of the three techniques. In Sec. II A a model system for the description of time-resolved Raman scattering with light that is modulated by a stochastic (Gauss-Markov) process will be given on which further calculations will be based. The properties of the RFD signal which are of most interest here are calculated in Sec. II B. Then in Sec. II C and II D the behavior of CSRS and TSRG is investigated and the section is concluded with a discussion of the theoretical results. Finally, in Sec. III the experimental observations of incoherent RFD with unamplified non-transform-limited mode-locked pulses on the 524-cm^{-1} mode of liquid CH_3I and the 656-cm^{-1} mode of liquid CS_2 are presented. The experimental results are in agreement with the theoretical predictions made in the first half of this paper and previous "conventional" studies. Furthermore the experiments indicate that it is possible to perform time-resolved Raman scattering studies with incoherent light using unamplified pulses in media that do not provide any intermediate resonance enhancement.

II. A UNIFIED DESCRIPTION OF RAMAN SCATTERING

In this paper Raman scattering with low intensity stochastic light is considered. In third-order perturbation theory (lowest order for Raman processes) there are four types of Raman processes: generation of anti-Stokes fields due to CARS (coherent anti-Stokes Raman scattering), of laser fields due to SRS (stimulated Raman scattering), of Stokes fields due to SRS, and finally of super-Stokes fields due to CSRS. The naming convention for the four types of field is shown in Fig. 1. Note the symmetry in these processes: CARS and CSRS have identical properties and the same holds for the two types of SRS. Below, in Sec. II A, a general framework for describing all these processes is presented, including the coherence properties of the fields involved in generation as well as detection. Then in Sec. II B, II C, and II D, RFD, incoherent CSRS, and TSRG are discussed.

A. General definitions

Coherent Raman scattering of incoherent light from a vibrational transition in the electronic ground state of a molecule will be considered. The molecular system will be treated as a simple three-level system with ground state $|1\rangle$, vibrationally excited state belonging to the ground state manifold of vibrational levels $|2\rangle$, and an electronically excited state $|3\rangle$. This system is described by the Hamiltonian

$$\hat{\mathcal{H}}_0=\sum_{i=1}^{3}\hbar\Omega_i\hat{\Pi}_{ii} \tag{1}$$

where $\hbar\Omega_i$ is the energy eigenvalue of state $|i\rangle$ and $\hat{\Pi}_{ij}=|i\rangle\langle j|$ is the state-flip operator. Transitions between states $|1\rangle$ and $|2\rangle$ are parity forbidden and transitions between $|1\rangle$ and $|3\rangle$, and $|2\rangle$ and $|3\rangle$ are allowed. All transitions are assumed to be homogeneously broadened with dephasing rate γ_{ij}, $i\neq j$ and population relaxation is neglected (and irrelevant for that matter). For all fields (which are taken to be scalar quantities in the equations) the coupling Hamiltonian is taken to be of the form (H.c. stands for Hermitian conjugate)

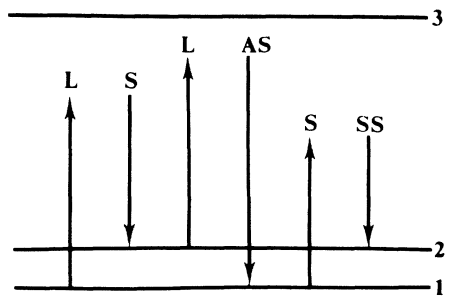

FIG. 1. The three-level system used in the text to describe Raman scattering and the naming convention for the fields. The abbreviations are L, laser; S, Stokes; AS, anti-Stokes; and SS, super-Stokes.

$$\hat{\mathcal{H}}_1=-\hat{\mu}E(t)$$
$$=-\frac{\mu}{2}\sum_{i=1,2}\sum_{j=L,S}\mathcal{E}_j(t)e^{-i(\omega_j t-\mathbf{k}_j\cdot\mathbf{r})}\hat{\Pi}_{3i}+\text{H.c.}, \tag{2}$$

with $\mu_{31}=\mu_{32}\equiv\mu$ the dipole moment matrix element, E_i the laser field strength and $\mathcal{E}_i(t)$ its slowly varying envelope.[25] The spatial dependence of $\hat{\mathcal{H}}_1$ will be suppressed in the following.

The evolution of the system is governed by the Liouville–von Neumann equation of motion for the density matrix $\hat{\rho}$ of the molecule,

$$\frac{d\hat{\rho}}{dt}=\left[\frac{\hat{\mathcal{H}}}{i\hbar},\hat{\rho}\right], \tag{3}$$

where $\hat{\mathcal{H}}$ is the total Hamiltonian $\hat{\mathcal{H}}_0+\hat{\mathcal{H}}_1$. The evolution of the matrix elements of $\hat{\rho}$ is readily calculated using the double Feynman diagrammatic technique.[26,27] The induced macroscopic polarization due to an interaction sequence is given by $P(t)=N\,\mathrm{Tr}(\hat{\mu}\hat{\rho})$. Due to the assumption of low intensity of the input fields and the additional assumption that the sample is optically thin, the generated electric field $E(t)$ is simply linearly proportional to $P(t)$.

For a given field $E(t)$ at a (quadratic) photodetector, the signal I is proportional to[28]

$$I(\omega)\propto\int_{-\infty}^{\infty}dT\,\langle E^*(t)E(t+T)\rangle e^{i\omega T-\gamma_{\text{slit}}|T|}, \tag{4a}$$

where γ_{slit} is the spectral width of the photodetector and the angled brackets denote a temporal average over the fields. For a photodetector with a very broad spectral response (white detector limit) Eq. (4a) can be approximated by

$$I\propto\langle|E(t)|^2\rangle\,. \tag{4b}$$

Note that the averaged quantity in Eq. (4b) is formally a two-particle single-time correlation function[29] that can be represented by "quadruple Feynman diagrams,"[30] although the spatial (or particle) dependence is not explicit here.

The fields that appear in the perturbative expansion of $P(t)$ will be assumed to be stationary zero-mean Gauss-Markov (GM) processes (i.e., an Ornstein-Uhlenbeck process[31]). The slowly varying envelopes of the fields are written as

$$\mathcal{E}_i(t)=\mathcal{A}(t)\epsilon_i(t),\quad i=L,S \tag{5}$$

where $\mathcal{A}(t)$ is a (deterministic) pulse envelope taken equal for the laser and Stokes fields, $\epsilon(t)$ is the GM process proper, and the indices L and S denote laser and Stokes, respectively. Furthermore

$$\langle\epsilon_i^*(t)\epsilon_j(t')\rangle=e^{-\Gamma_i|t-t'|}\delta_{ij}\,, \tag{6}$$

$\mathcal{A}(t)$ is assumed to be uncorrelated with $\epsilon_i(t)$ and is tak-

en of the form

$$\mathcal{A}(t)=e^{-\Gamma_P|t|} \tag{7}$$

where Γ_P is the pulse width. In the case of cw fields the limit $\Gamma_P=0$ is taken. Although the average over $\epsilon(t)$ has now become an average over an ensemble of stochastic processes, the average over $\mathcal{A}(t)$ is still a temporal average.

B. Incoherent RFD

The idea of RFD is relatively recent and it was discussed by Felker and co-workers[24,32–34] and others.[35–37] A complete theory, however, for (partially) incoherent fields was never given and will be given below. Consider the double Feynman diagram in Fig. 2 for CARS; this diagram corresponds to the following expression for the CARS polarization:

$$P^{(3)}(t)=C\int_{-\infty}^{t}dt_3\int_{-\infty}^{t_3}dt_2\int_{-\infty}^{t_2}dt_1\mathcal{E}_L(t_1)\mathcal{E}_S^*(t_2)\mathcal{E}_L(t_3)\times\exp[-i\omega_{\mathrm{AS}}t-(\gamma_{31}+i\Delta_1)(t_2-t_1)-(\gamma+i\Delta)(t_3-t_2)-(\gamma_{31}+i\Delta_2)(t-t_3)] \tag{8a}$$

where

$$\begin{aligned}
&\Delta_1=\Omega_{31}-\omega_L\ ,\\
&\Delta=\Omega_{21}-\omega_L+\omega_S\ ,\\
&\Delta_2=\Omega_{31}-\omega_L+\omega_S-\omega_L\ ,\\
&\Omega_{ij}=\Omega_i-\Omega_j\ ,\\
&\omega_{\mathrm{AS}}=2\omega_L-\omega_S\ ,\\
&\gamma=\gamma_{21}\ ,\\
&C=-iN\mu^4/4\hbar^3\ ,
\end{aligned} \tag{8b}$$

and ω_{AS} is the anti-Stokes frequency. Note that the propagators over the intervals t_2-t_1 and $t-t_3$ become proportional to Dirac δ functions as the detuning with the intermediate resonance tends to infinity.

Now the difference between CARS and RFD (see Fig. 3) lies in the fact that in RFD the probe pulse is replaced by a probe-pulse pair consisting of laser and Stokes pulses. Mathematically, the replacements

$$\begin{aligned}
&\mathcal{E}_L(t)\rightarrow\mathcal{E}_1(t)+\mathcal{E}_3(t)\rightarrow\mathcal{E}_L(t)+\mathcal{E}_L(t-\tau)e^{+i\omega_L\tau}\ ,\\
&\mathcal{E}_S(t)\rightarrow\mathcal{E}_2(t)+\mathcal{E}_4(t)\rightarrow\mathcal{E}_S(t)+\mathcal{E}_S(t-\tau)e^{+i\omega_S\tau}
\end{aligned} \tag{9}$$

are made in Eq. (8), where τ is the delay between the excitation and probe-pulse pairs, resulting in eight different terms. We write

$$\begin{aligned}
P^{(3)}(t)=Ce^{-i\omega_{\mathrm{AS}}t}\int_{-\infty}^{t}dt'e^{-\phi(t-t')}\{&\mathcal{E}_L(t')\mathcal{E}_S^*(t')\mathcal{E}_L(t-\tau)\exp(+i\omega_L\tau)\\
&+\mathcal{E}_L(t'-\tau)\mathcal{E}_S^*(t')\mathcal{E}_L(t)\exp(+i\omega_L\tau)\\
&+\mathcal{E}_L(t')\mathcal{E}_S^*(t'-\tau)\mathcal{E}_L(t-\tau)\exp[+i(\omega_L-\omega_S)\tau]\\
&+\mathcal{E}_L(t'-\tau)\mathcal{E}_S^*(t'-\tau)\mathcal{E}_L(t)\exp[+i(\omega_L-\omega_S)\tau]+\mathcal{E}_L(t')\mathcal{E}_S^*(t')\mathcal{E}_L(t)\\
&+\mathcal{E}_L(t'-\tau)\mathcal{E}_S^*(t')\mathcal{E}_L(t-\tau)\exp(+i2\omega_L\tau)\\
&+\mathcal{E}_L(t')\mathcal{E}_S^*(t'-\tau)\mathcal{E}_L(t)\exp(-i\omega_S\tau)\\
&+\mathcal{E}_L(t'-\tau)\mathcal{E}_S^*(t'-\tau)\mathcal{E}_L(t-\tau)\exp[+i(2\omega_L-\omega_S)\tau]\}
\end{aligned} \tag{10}$$

where $\phi=\gamma+i\Delta$. Consequently the expression for the intensity of the RFD signal, which is proportional to the absolute square of Eq. (10), contains 64 terms. Concentrating on that part of the signal that oscillates slowly as a function of the delay τ, it is found

$$\langle E^*(t)E(t+T)\rangle \propto e^{-i\omega_{AS}T}\int_{-\infty}^{t+T}dt'\int_{-\infty}^{t}dt''\exp[-\phi(t+T-t')-\phi^*(t-t'')]$$
$$\times\{\langle \mathcal{E}_L(t')\mathcal{E}_S^*(t')\mathcal{E}_L(t+T-\tau)\mathcal{E}_L^*(t''-\tau)\mathcal{E}_S(t''-\tau)\mathcal{E}_L^*(t-\tau)\rangle e^{-i\Omega\tau}$$
$$+\langle \mathcal{E}_L(t'-\tau)\mathcal{E}_S^*(t'-\tau)\mathcal{E}_L(t+T-\tau)\mathcal{E}_L^*(t'')\mathcal{E}_S(t'')\mathcal{E}_L^*(t-\tau)\rangle e^{+i\Omega\tau}$$
$$+\langle \mathcal{E}_L(t'-\tau)\mathcal{E}_S^*(t')\mathcal{E}_L(t+T)\mathcal{E}_L^*(t''-\tau)\mathcal{E}_S(t''-\tau)\mathcal{E}_L^*(t-\tau)\rangle e^{-i\Omega\tau}$$
$$+\langle \mathcal{E}_L(t'-\tau)\mathcal{E}_S^*(t'-\tau)\mathcal{E}_L(t+T-\tau)\mathcal{E}_L^*(t''-\tau)\mathcal{E}_S(t'')\mathcal{E}_L^*(t)\rangle e^{+i\Omega\tau}$$
$$+\langle \mathcal{E}_L(t')\mathcal{E}_S^*(t'-\tau)\mathcal{E}_L(t+T-\tau)\mathcal{E}_L^*(t'')\mathcal{E}_S(t'')\mathcal{E}_L^*(t)\rangle e^{+i\Omega\tau}$$
$$+\langle \mathcal{E}_L(t')\mathcal{E}_S^*(t')\mathcal{E}_L(t+T)\mathcal{E}_L^*(t'')\mathcal{E}_S(t''-\tau)\mathcal{E}_L^*(t-\tau)\rangle e^{-i\Omega\tau}$$
$$+\langle \mathcal{E}_L(t'-\tau)\mathcal{E}_S^*(t'-\tau)\mathcal{E}_L(t+T)\mathcal{E}_L^*(t'')\mathcal{E}_S(t'')\mathcal{E}_L^*(t)\rangle e^{+i\Omega\tau}$$
$$+\langle \mathcal{E}_L(t')\mathcal{E}_S^*(t')\mathcal{E}_L(t+T)\mathcal{E}_L^*(t''-\tau)\mathcal{E}_S(t''-\tau)\mathcal{E}_L^*(t)\rangle e^{-i\Omega\tau}\} \quad (11)$$

where $\Omega=\omega_L-\omega_S$. It may be clear that Ω is the main frequency of the Raman fringes.

There are various useful options: either the laser or Stokes field may be incoherent, the fields may be cw or pulsed, the linear polarization may be varied and finally the detection of the signal may be broadband or pseudomonochromatic. These will be discussed below.

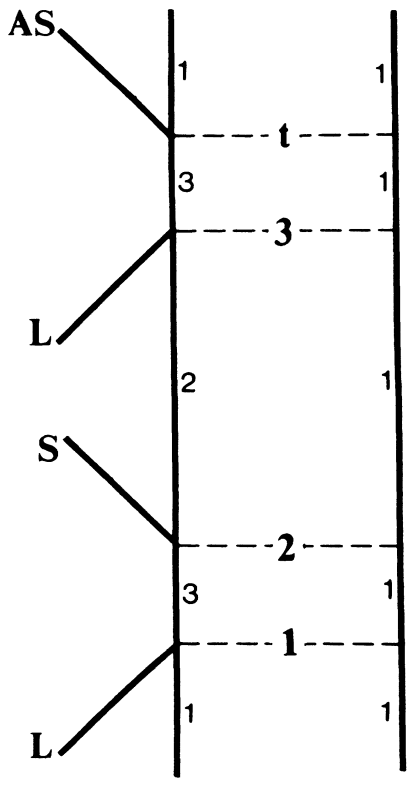

FIG. 2. The basic process of RFD is the generation of an anti-Stokes field by two fields at the laser frequency and one at the Stokes frequency, $\omega_{AS}=2\omega_L-\omega_S$. With $E_L=E_1$ or E_3 and $E_S=E_2$ or E_4 (see Fig. 3) this diagram stands for eight different equations.

1. *Stochastic laser cw fields and broadband detection*

In the case of broadband detection the signal is proportional to $\langle|E(t)|^2\rangle$ and if the fields are polarized parallel to each other (i.e., $\mathbf{E}_1\|\mathbf{E}_2\|\mathbf{E}_3\|\mathbf{E}_4$) and only the laser fields incoherent, it is found that

$$I\propto(\alpha+i\beta)(\tau)e^{-i\Omega\tau}+\text{c.c.}, \quad (12)$$

where

$$\alpha=e^{-\gamma|\tau|}[\mathfrak{X}\cos(\Delta\tau)+\mathfrak{Y}\sin(\Delta|\tau|)]+\mathfrak{Z}e^{-\Gamma_L|\tau|},$$
$$\beta=e^{-\gamma|\tau|}\left[\mathfrak{Y}\frac{\tau}{|\tau|}\cos(\Delta\tau)-\mathfrak{X}\sin(\Delta\tau)\right]$$
$$-\mathfrak{Y}\frac{\tau}{|\tau|}e^{-\Gamma_L|\tau|}, \quad (13)$$

and

$$\mathfrak{X}=\mathcal{N}_L\Gamma_L[(\Gamma_L-\gamma)(\Gamma_L+3\gamma)+\Delta^2],$$
$$\mathfrak{Y}=\mathcal{N}_L4\gamma\Gamma_L\Delta,$$
$$\mathfrak{Z}=\mathcal{N}_L(\Gamma_L-\gamma)(\Gamma_L^2-\gamma\Gamma_L-4\gamma^2)+\Delta^2(\Gamma_L+4\gamma), \quad (14)$$
$$\mathcal{N}_i^{-1}=\gamma|\Gamma_i-\phi|^2|\Gamma_i+\phi|^2,\quad i=L,S.$$

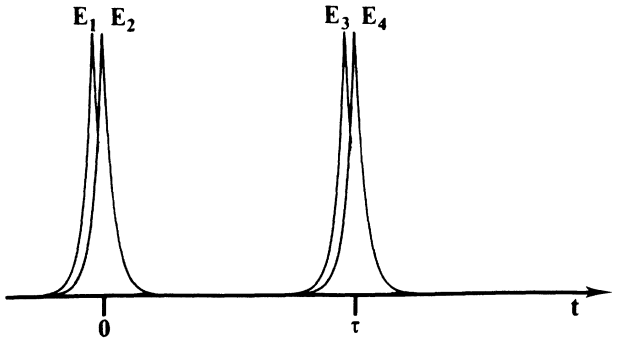

FIG. 3. In all experiments described here the delayed fields (E_3 and E_4) are exact replicas of the other fields (E_1 and E_2, respectively) except for a phase factor. The assignment of the actual central frequency (i.e., laser or Stokes) depends on the process considered.

To find a measure of the fringe amplitude from Eq. (12), two coordinates are defined as

$$x \equiv I\cos(\Omega_{21}\tau) \cong \alpha\cos(\Delta\tau) - \beta\sin(\Delta\tau) ,$$
$$y \equiv I\sin(\Omega_{21}\tau) \cong \alpha\sin(\Delta\tau) + \beta\cos(\Delta\tau) . \tag{15}$$

Then the amplitude is given by $(x^2+y^2)^{1/2}$, where the high-frequency components are filtered out.

In the case of orthogonal linear polarization of the first arriving fields with respect to the delayed fields (thus, cf. Fig. 3, $\mathbf{E}_1 \| \mathbf{E}_2$, $\mathbf{E}_3 \| \mathbf{E}_4$, $\mathbf{E}_1 \perp \mathbf{E}_3$), the signal is again of the form of Eq. (12). It is found for $\tau \geq 0$

$$\alpha = e^{-\gamma\tau}[\mathfrak{A}\cos(\Delta\tau) - \mathfrak{B}\sin(\Delta\tau)] + \mathfrak{C}e^{-\Gamma_L\tau} ,$$
$$\beta = e^{-\gamma\tau}[-\mathfrak{B}\cos(\Delta\tau) - \mathfrak{A}\sin(\Delta\tau)] - \mathfrak{B}e^{-\Gamma_L\tau} , \tag{16a}$$

and for $\tau < 0$

$$\alpha = e^{\gamma\tau}[\mathfrak{D}\cos(\Delta\tau) - \tfrac{1}{2}\mathfrak{B}\sin(\Delta\tau)] + \mathfrak{E}e^{\Gamma_L\tau} ,$$
$$\beta = e^{\gamma\tau}[-\tfrac{1}{2}\mathfrak{B}\cos(\Delta\tau) - \mathfrak{D}\sin(\Delta\tau)] + \tfrac{1}{2}\mathfrak{B}e^{\Gamma_L\tau} , \tag{16b}$$

where

$$\mathfrak{A} = \mathcal{N}_L\{\Gamma_L[(\Gamma_L-\gamma)(\Gamma_L+3\gamma)+\Delta^2]\} ,$$
$$\mathfrak{B} = \mathcal{N}_L(4\gamma\Gamma_L\Delta) ,$$
$$\mathfrak{C} = \mathcal{N}_L\{-2\gamma[(\Gamma_L-\gamma)(\Gamma_L+\gamma)-\Delta^2]\} , \tag{17}$$
$$\mathfrak{D} = \mathcal{N}_L[\Gamma_L(\Gamma_L^2-\gamma^2+\Delta^2)] ,$$
$$\mathfrak{E} = \mathcal{N}_L[2\gamma(\gamma^2+\Delta^2-\Gamma_L\gamma)] .$$

In the derivation of this equation it is crucial that all transition dipole moments are parallel (i.e., $\boldsymbol{\mu}_{13} \| \boldsymbol{\mu}_{23}$) and that orientational dynamics[38,39] have been neglected.

2. Stochastic Stokes cw fields and broadband detection

Making similar assumptions to those in Sec. II B 1, it is found for both polarization conditions [with Eq. (12)]

$$\alpha = e^{-\gamma|\tau|}[\mathfrak{A}\cos(\Delta\tau) + \mathfrak{B}\sin(\Delta|\tau|)] + \mathfrak{C}e^{-\Gamma_S|\tau|} ,$$
$$\beta = e^{-\gamma|\tau|}\left[\mathfrak{B}\frac{\tau}{|\tau|}\cos(\Delta\tau) - \mathfrak{A}\sin(\Delta\tau)\right] - \mathfrak{B}\frac{\tau}{|\tau|}e^{-\Gamma_S|\tau|} \tag{18}$$

where

$$\mathfrak{A} \equiv \mathcal{N}_S^{-1}\{\Gamma_S[\Delta^2+(\Gamma_S^2-\gamma^2)]\} ,$$
$$\mathfrak{B} \equiv \mathcal{N}_S^{-1}(2\gamma\Gamma_S\Delta) , \tag{19}$$
$$\mathfrak{C} \equiv \mathcal{N}_S^{-1}\{\gamma[\Delta^2-(\Gamma_S^2-\gamma^2)]\} .$$

3. Pulsed fields and broadband detection

As indicated in Sec. II A, in the case of pulsed fields the deterministic part of the field is decorrelated from the stochastic part. For stochastic laser as well as for stochastic Stokes pulses and for both polarization conditions, the signal can be expressed in the form of Eq. (12). Unfortunately the analytic expressions that result for the coefficients $\alpha(\tau)$ and $\beta(\tau)$ occupy several pages and cannot be given here for obvious reasons.[40] It suffices to state here that the form of the signal does not essentially change for pulse widths larger than the relaxation time. Naturally it has been checked that the mentioned equations reduce to their cw fields form discussed in the preceding subsections, for $\Gamma_P \to 0$.

4. Stochastic laser cw fields and monochromatic detection

As discussed above, the signal in the monochromatic limit is given by[28,41]

$$I \propto \int_{-\infty}^{\infty} dT \langle E^*(t)E(t+T)\rangle e^{i\omega_{AS}T} e^{-i\delta T - \gamma_{slit}|T|} , \tag{20}$$

where

$$\delta \equiv \omega_{AS} - \omega .$$

Note that the $e^{i\omega_{AS}T}$ term cancels the one in $\langle E^*(t)E(t+T)\rangle$. It turns out that there is only a measurable effect of the introduction of a limited spectral response of the photodetector if the polarization is parallel. Then

$$I(T,\tau) \propto (C_\alpha + C_\beta + C_\gamma + C_\delta)(\tau)e^{-i\Omega\tau} + \text{c.c.} \tag{21}$$

[This equation is of course again of the form of Eq. (12)] where

$$C_\alpha = e^{-\Gamma_L|T|}[H(x)(\mathfrak{M}e^{-\phi x} + \mathfrak{N}e^{-\Gamma_L x}) + H(-x)(\mathfrak{M}^*e^{\phi^* x} + \mathfrak{N}^*e^{\Gamma_L x})] , \tag{22a}$$

$$C_\beta = [H(T)\mathfrak{P}e^{-\Gamma_L T} + H(-T)(\mathfrak{Q}e^{\phi^* T} + \mathfrak{R}e^{\Gamma_L T})] \times [H(-x)\mathfrak{P}^*e^{\Gamma_L x} + H(x)(\mathfrak{Q}^*e^{-\phi x} + \mathfrak{R}^*e^{-\Gamma_L x})] , \tag{22b}$$

$$C_\gamma = e^{-\Gamma_L|x|}[H(T)(\mathfrak{M}e^{-\phi T} + \mathfrak{N}e^{-\Gamma_L T}) + H(-T)(\mathfrak{M}^*e^{\phi^* T} + \mathfrak{N}^*e^{\Gamma_L T})] , \tag{22c}$$

$$C_\delta = [H(x)\mathfrak{P}e^{-\Gamma_L x} + H(-x)(\mathfrak{Q}e^{\phi^* x} + \mathfrak{R}e^{\Gamma_L x})] \times [H(-T)\mathfrak{P}^*e^{\Gamma_L T} + H(T)(\mathfrak{Q}^*e^{-\phi T} + \mathfrak{R}^*e^{-\Gamma_L T})] , \tag{22d}$$

and

$$x \equiv T + \tau ,$$
$$H(t) \equiv \begin{cases} 0, & t<0 \\ 1, & t \geq 0 \end{cases}$$
$$\mathfrak{M} \equiv \mathcal{N}_L^{-1}[\Gamma_L(\Gamma_L^2-\gamma^2+\Delta^2+i2\gamma\Delta)] ,$$
$$\mathfrak{N} \equiv \mathcal{N}_L^{-1}(\Delta^2-\Gamma_L^2+\gamma^2-i2\gamma\Gamma_L\Delta) , \tag{23}$$
$$\mathfrak{P} \equiv (\phi^*+\Gamma_L)^{-1} ,$$
$$\mathfrak{Q} \equiv (\phi^*+\Gamma_L)^{-1} + (\Gamma_L-\phi^*)^{-1} ,$$
$$\mathfrak{R} \equiv (\phi^*-\Gamma_L)^{-1} .$$

The Fourier transform is easily calculated by using convolution integrals; these integrals can be analytically solved via Jordan's lemma and complex contour integration, yielding finally

$$C_\alpha = 2[(\mathfrak{M}+\mathfrak{M}^*)I_{ff}(0,\Gamma'_L,\delta+\Delta,\gamma) - i(\mathfrak{M}-\mathfrak{M}^*)I_{fg}(0,\Gamma'_L,\delta+\Delta,\gamma) + (\mathfrak{N}+\mathfrak{N}^*)I_{ff}(0,\Gamma'_L,\delta,\Gamma_L) - i(\mathfrak{N}-\mathfrak{N}^*)I_{fg}(0,\Gamma'_L,\delta,\Gamma_L)] , \tag{24a}$$

$$\begin{aligned} C_\beta = {} & |\mathfrak{P}+\mathfrak{R}|^2 I_{ff}(0,\Gamma'_L,\delta,\Gamma_L) + |\mathfrak{P}-\mathfrak{R}|^2 I_{gg}(0,\Gamma'_L,\delta,\Gamma_L) + |\mathfrak{Q}|^2 I_{ff}(\Delta,\gamma',\delta+\Delta,\gamma) \\ & + |\mathfrak{Q}|^2 I_{gg}(\Delta,\gamma',\delta+\Delta,\gamma) + i(\mathfrak{P}+\mathfrak{R})(\mathfrak{P}^*-\mathfrak{R}^*)I_{fg}(0,\Gamma'_L,\delta,\Gamma_L) - i(\mathfrak{P}^*+\mathfrak{R}^*)(\mathfrak{P}-\mathfrak{R})I_{gf}(0,\Gamma'_L,\delta,\Gamma_L) \\ & + \mathfrak{Q}^*(\mathfrak{P}+\mathfrak{R})I_{ff}(0,\Gamma'_L,\delta+\Delta,\gamma) + \mathfrak{Q}(\mathfrak{P}^*+\mathfrak{R}^*)I_{ff}(\Delta,\gamma',\delta,\Gamma_L) - i\mathfrak{Q}^*(\mathfrak{P}+\mathfrak{R})I_{fg}(0,\Gamma'_L,\delta+\Delta,\gamma) \\ & + i\mathfrak{Q}(\mathfrak{P}^*+\mathfrak{R}^*)I_{gf}(\Delta,\gamma',\delta,\Gamma_L) - i\mathfrak{Q}^*(\mathfrak{P}-\mathfrak{R})I_{gf}(0,\Gamma'_L,\delta+\Delta,\gamma) + i\mathfrak{Q}(\mathfrak{P}^*-\mathfrak{R}^*)I_{fg}(\Delta,\gamma',\delta,\Gamma_L) \\ & - \mathfrak{Q}^*(\mathfrak{P}-\mathfrak{R})I_{gg}(0,\Gamma'_L,\delta+\Delta,\gamma) - \mathfrak{Q}(\mathfrak{P}^*-\mathfrak{R}^*)I_{gg}(\Delta,\gamma',\delta,\Gamma_L) - i|\mathfrak{Q}|^2 I_{fg}(\Delta,\gamma',\delta+\Delta,\gamma) + i|\mathfrak{Q}|^2 I_{gf}(\Delta,\gamma',\delta+\Delta,\gamma) . \end{aligned} \tag{24b}$$

C_γ and C_δ are given by the same expressions as given above in Eq. (24) for C_α and C_β, except that I_{ff}, I_{fg}, I_{gf}, and I_{gg} should be replaced by I'_{ff}, I'_{fg}, I'_{gf}, and I'_{gg}, where

$$I_{ij}(\Omega_1,a,\Omega_2,b) = [H(\tau)x_{ij} + H(-\tau)x_{ij}^*]e^{i(\delta+\Omega_1)\tau - a|\tau|} + [H(\tau)y_{ij} + H(-\tau)y_{ij}^*]e^{i(\delta-\Omega_2)\tau - b|\tau|} , \tag{25a}$$

$$I'_{ij}(\Omega_1,a,\Omega_2,b) = [H(\tau)x_{ij}^* + H(-\tau)x_{ij}]e^{-i\Omega_1\tau - a|\tau|} + [H(\tau)y_{ij}^* + H(-\tau)y_{ij}]e^{i\Omega_2\tau - b|\tau|}, \quad i,j = f,g , \tag{25b}$$

$$x_{ff} = \frac{\pi b}{[\Omega_1+\Omega_2+i(a-b)][\Omega_1+\Omega_2+i(a+b)]}, \quad y_{ff} = \frac{\pi a}{[\Omega_1+\Omega_2+i(a-b)][\Omega_1+\Omega_2-i(a+b)]} ,$$

$$x_{fg} = \frac{\pi(\Omega_1+\Omega_2+ia)}{[\Omega_1+\Omega_2+i(a-b)][\Omega_1+\Omega_2+i(a+b)]}, \quad y_{fg} = \frac{i\pi a}{[\Omega_1+\Omega_2+i(a-b)][\Omega_1+\Omega_2-i(a+b)]} ,$$

$$x_{gf} = \frac{-i\pi b}{[\Omega_1+\Omega_2+i(a-b)][\Omega_1+\Omega_2+i(a+b)]}, \quad y_{gf} = \frac{\pi(\Omega_1+\Omega_2-ib)}{[\Omega_1+\Omega_2+i(a-b)][\Omega_1+\Omega_2-i(a+b)]} ,$$

$$x_{gg} = \frac{-i\pi(\Omega_1+\Omega_2+ia)}{[\Omega_1+\Omega_2+i(a-b)][\Omega_1+\Omega_2+i(a+b)]}, \quad y_{gg} = \frac{i\pi(\Omega_1+\Omega_2-ib)}{[\Omega_1+\Omega_2+i(a-b)][\Omega_1+\Omega_2-i(a+b)]} ,$$

and

$$\Gamma'_L \equiv \Gamma_L + \gamma_{\text{slit}}, \quad \gamma' \equiv \gamma + \gamma_{\text{slit}} .$$

C. Incoherent CSRS

The theory of incoherent CSRS has been extensively discussed in Ref. 22, therefore it will be discussed only briefly here. Note that incoherent CSRS is very similar to RFD described above, the difference being that the signal is generated at the super-Stokes frequency and the probe pulse consists of a Stokes pulse only. This corresponds to the replacements

$$\begin{aligned} & \mathcal{E}_L(t) \leftrightarrow \mathcal{E}_1(t) , \\ & \mathcal{E}_S(t) \rightarrow \mathcal{E}_2(t) + \mathcal{E}_3(t) \rightarrow \mathcal{E}_S(t) + \mathcal{E}_S(t-\tau)e^{+i\omega_S\tau} \end{aligned} \tag{26}$$

(see the double Feynman diagrams in Fig. 4). Only the signal for cw incoherent light, a stochastic Stokes field (a stochastic laser field has no beneficial effects), and parallel polarization ($\mathbf{E}_1 \| \mathbf{E}_2 \| \mathbf{E}_3$) will be discussed. Furthermore it will be assumed that the intermediate electronic state $|3\rangle$ is excited far off resonance (in Ref. 22 the resonant case is also discussed). It will, however, not be assumed *a priori* that the laser and Stokes fields are two-photon resonant with the transition $|1\rangle$-$|2\rangle$. Then the average incoherent CSRS intensity is found to be given by (cf. Ref. 22)

$$I(\tau) \propto \int_{-\infty}^{t}\int_{-\infty}^{t} dt'dt'' e^{-\phi(t-t')-\phi^*(t-t'')}\langle [E_S^*(t)E_S^*(t'-\tau) + E_S^*(t-\tau)E_S^*(t')][E_S(t)E_S(t''-\tau) + E_S(t-\tau)E_S(t'')]\rangle \tag{27}$$

where $\phi \equiv \gamma + i\Delta$, γ is the dephasing rate of the transition $|1\rangle$-$|2\rangle$, $\Delta \equiv \Omega_{21} - \omega_L + \omega_S$ is the two-photon detuning. Using Eqs. (26) and (27) the CSRS intensity is easily found:

$$\begin{aligned} I \propto {} & \mathcal{N}_S^{-1} 2(2\gamma+\Gamma_S)|\Gamma_S - \phi|^2 + e^{-2\Gamma_S|\tau|}\mathcal{N}_S^{-1} 4\gamma(\gamma^2+\Delta^2) + e^{-2\gamma|\tau|}\mathcal{N}_S^{-1} 4\gamma\Gamma_S^2 \\ & + e^{(-\Gamma_S-\gamma)|\tau|}\cos(\Delta|\tau|)\mathcal{N}_S^{-1} 2\Gamma_S[(\Gamma_S+\gamma)(\Gamma_S-3\gamma)+\Delta^2] + e^{(-\Gamma_S-\gamma)|\tau|}\sin(\Delta|\tau|)\mathcal{N}_S^{-1} 8\gamma\Gamma_S\Delta . \end{aligned} \tag{28}$$

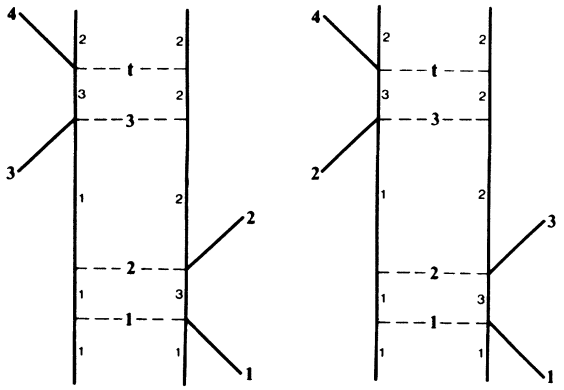

FIG. 4. With $E_L=E_1$, $E_S=E_2$ or E_3, and $E_4=0$, the basic CSRS diagram yields these two diagrams that both give the phase-matching condition $\mathbf{k}_4=\mathbf{k}_3+\mathbf{k}_2-\mathbf{k}_1$.

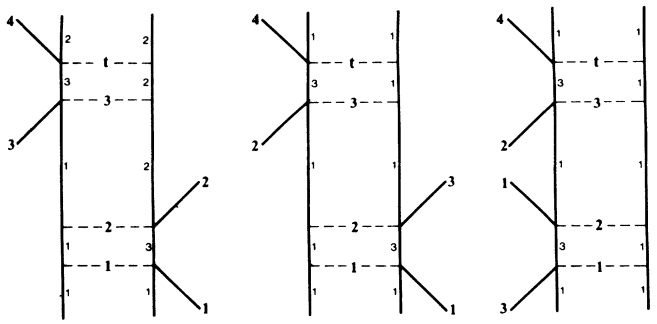

FIG. 5. With $E_L=E_1$ or E_3 and $E_S=E_2$ or E_4 and imposing the phase-matching condition $\mathbf{k}_4=\mathbf{k}_3+\mathbf{k}_2-\mathbf{k}_1$ leads to these three double Feynman diagrams. Diagram (a) is the usual SRS process; diagrams (b) and (c) are of an electronic character.

For $\Delta=0$ Eq. (28) reduces to the result of Ref. 22. Note that in contrast to RFD, there are no fringes.

D. Incoherent TSRG

TSRG was developed by Heritage[42] and extensively discussed by Van Exter *et al.*[23,43,44] and others.[45] For consistency TSRG will be discussed in the same framework as CSRS and RFD above. The pulse sequence of TSRG is identical to that of RFD and the replacement Eq. (9) can be used. However, in TSRG the signal is detected at the Stokes frequency. Usually in the experiments the phase matching is chosen in such a way that the signal is observed in the direction of the Stokes frequency part of the probe-pulse pair. Due to the frequency degeneracy of TSRG there are three diagrams (see Fig. 5) that contribute to the signal in the above-mentioned phase-matched direction. Only one of them is of Raman type, the other two are of electronic origin and do not occur in either CSRS or CARS. From the double Feynman diagrams in Fig. 5 the third-order polarization is found to be given by (under the same assumptions as in the preceding sections)

$$P^{(3)}(t)=C\int_{-\infty}^{t}dt'e^{-\phi^*(t-t')-i\omega_S t}\mathcal{E}_1^*(t')\mathcal{E}_2(t')\mathcal{E}_3(t)+C\int_{-\infty}^{t}dt'2e^{-i\omega_S t}\mathcal{E}_1^*(t')\mathcal{E}_3(t')\mathcal{E}_2(t) \quad (29)$$

where C and ϕ are defined as before. Note that Eq. (29) has been written in such a way that the explicit frequency dependence is identical to the Stokes frequency ($\omega_L-\omega_S-\omega_L=-\omega_S$). Indeed TSRG is detected by heterodyne techniques,[46,47] with the delayed Stokes pulse (E_4) acting as the local oscillator. The average heterodyne signal $\langle w\rangle$ can be expressed as

$$\langle w\rangle\propto\left\langle \mathrm{Re}\int_{-\infty}^{t}dt'e^{-\phi^*(t-t')-i(\omega_L-\omega_S)\tau}\mathcal{E}_L^*(t')\mathcal{E}_S(t')\mathcal{E}_L(t-\tau)\mathcal{E}_S^*(t-\tau)\right\rangle + \left\langle \mathrm{Re}\int_{-\infty}^{t}dt'2e^{-i(\omega_L-\omega_S)\tau}\mathcal{E}_L^*(t')\mathcal{E}_L(t')\mathcal{E}_S(t-\tau)\mathcal{E}_S^*(t-\tau)\right\rangle . \quad (30)$$

In contrast to the short discussion of CSRS in the preceding section, it will be assumed that both laser and Stokes fields are independent GM random processes and furthermore that both fields are pulsed. Using the equations from Sec. II A, it is found from the "Raman part" of Eq. (30) for negative delay ($\tau<0$)

$$\langle w\rangle\propto\mathrm{Re}\exp[-i(\omega_L-\omega_S)\tau+\mathcal{S}\tau]\times\{(\phi+\mathcal{S})^{-2}+[2\Gamma_P(\phi+\mathcal{S})]^{-1}+[2\Gamma_P(\phi-\mathcal{D})]^{-1}-[(\phi-\mathcal{D})(\phi+\mathcal{S})]^{-1}-\tau(\phi+\mathcal{S})^{-1}\} \quad (31a)$$

and for positive delay ($\tau>0$)

$$\begin{aligned}\langle w\rangle\propto{}&\mathrm{Re}\exp[-i(\omega_L-\omega_S)\tau]\\&\times(\exp(-\phi\tau)\{(\phi+\mathcal{S})^{-2}-[2\Gamma_P(\phi-\mathcal{S})]^{-1}+[2\Gamma_P(\phi+\mathcal{S})]^{-1}-[(\phi-\mathcal{D})(\phi+\mathcal{S})]^{-1}\\&\quad-[(\phi+\mathcal{D})(\phi-\mathcal{S})]^{-1}+[2\Gamma_P(\phi-\mathcal{D})]^{-1}-[2\Gamma_P(\phi+\mathcal{D})]^{-1}\}\\&+\exp(-\mathcal{S}\tau)\{-(\phi-\mathcal{S})^{-2}+[2\Gamma_P(\phi-\mathcal{S})]^{-1}+[2\Gamma_P(\phi+\mathcal{D})]^{-1}\\&\quad+[(\phi+\mathcal{D})(\phi-\mathcal{S})]^{-1}+\tau(\phi-\mathcal{S})^{-1}\})\end{aligned} \quad (31b)$$

and from the "electronic part" of Eq. (30)

$$\langle w \rangle \propto \cos(\Omega\tau)e^{-\mathcal{S}|\tau|}(|\tau|+\Gamma_P)^2 \tag{31c}$$

where

$$\mathcal{S}\equiv\Gamma_P+\Gamma_L+\Gamma_S \text{ and } \mathcal{D}\equiv\Gamma_P-\Gamma_L-\Gamma_S \ .$$

Again there are fringes with the same main frequency as in RFD. An estimate of the fringe amplitude is obtained in a way similar to the case of incoherent RFD [cf. Eq. (15)].

E. Discussion of results

The reason that CSRS and TSRG as well as RFD have been discussed may be clear: the respective techniques are very similar. The reason seems to be that all three techniques rely on some sort of homodyne or heterodyne detection scheme: a relevant signal modulates a background. This background consists of two- and four-beam CARS in the case of RFD, the uncorrelated parts of the Stokes field generating a constant signal in CSRS and an externally supplied Stokes beam in the case of TSRG. Furthermore, the temporal resolution is in all techniques determined by the inverse of the spectral width of the pulses, rather than their actual temporal width. The specific properties of the three techniques will be discussed below.

Incoherent RFD is generated by the interference of a decaying and a nondecaying component of the anti-Stokes field. As a result of this homodyne scheme (Fig. 6 shows the result for stochastic laser, parallel excitation, and cw fields), the RFD signal decays twice as slowly as a decay measured with ordinary CARS or CSRS. As discussed in Ref. 22, two extreme cases can be considered. The case $\Gamma/\gamma \gg 1$, when the tail of the signal decays with γ [that is with $(T_2)^{-1}$, where T_2 is the usual transverse relaxation time], and $\Gamma_i/\gamma \ll 1$, when the signal reduces to the two-point intensity autocorrelation function of the ith field (where $i=L,S$). As can be seen in the figure, it seems that as the coherence time decreases, the height of the coherence spike converges to a constant.

As the two-photon detuning from Raman resonance is increased (see Figs. 7 and 8) small beats emerge. In the case of a stochastic Stokes field the beats are so small as to render them experimentally unobservable. In all cases one expects a spikelike feature rather than beats as such if the signal-to-noise ratio in the experiment is low. The calculations in the pseudomonochromatic limit, however, show that this spikes turns into full blown beats as the slit width is decreased (Fig. 9).

Careful examination of the theoretical predictions in the pseudomonochromatic limit suggests the following rules. Part of the signal oscillates as function of the delay τ at angular frequency $\Omega_{21}+(\Delta-\gamma)$ while another part of the signal oscillates with frequency $[\Omega_{21}+(\Delta-\gamma)]-(2\Delta+\delta)$. The interference of these two components leads to beats in the total signal at the frequency $2\Delta+\delta$. For large two-photon detunings ($\delta > -\Delta$ for positive Δ and $\delta < -\Delta$ for negative Δ) a third frequency appears, namely just Ω_{21}. Note that in the pseudomonochromatic limit there are always beats at $2\Delta+\delta$, thus beats can be even be expected if the vibration of the molecule is excited on resonance ($\Delta=0$) but the detection frequency is detuned ($\delta\neq 0$). The result that the beat frequency depends on the detection center frequency is not so surprising considering the fact that the signal is homo-

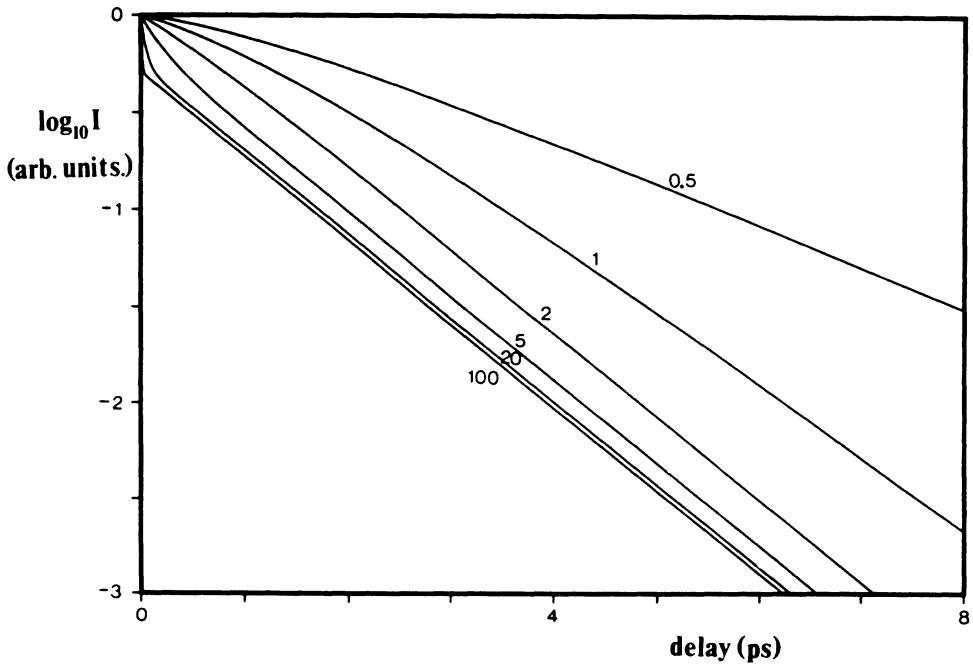

FIG. 6. Normalized incoherent RFD signal intensity in the parallel configuration with cw fields ($\Gamma_P=0$) and broadband detection, plotted as a function of the delay τ. The coherence rate Γ_L of the laser field varies from 0.5 to 100 ps^{-1} and $\gamma=1$ ps^{-1}.

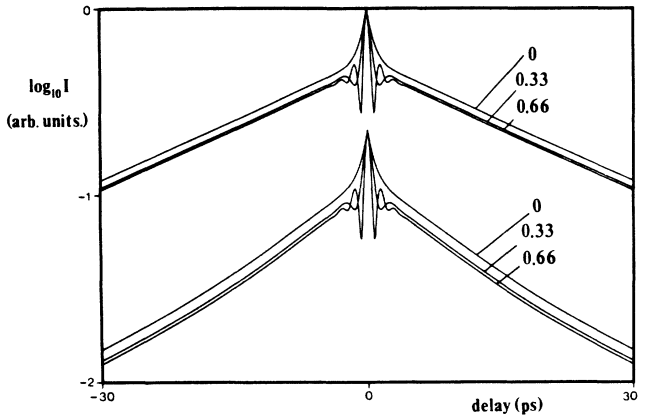

FIG. 7. Normalized RFD signal with broadband detection and parameter values $\Gamma_L=1.42$, $\gamma=0.05$, and $\Delta=0.0$, 0.333, and 0.666 (all in ps^{-1}) and parallel polarization configuration. In the upper traces cw fields have been assumed ($\Gamma_P=0$) and in the lower traces $\Gamma_P=0.1$ ps^{-1}.

dyne detected. In the white detector limit the oscillation at frequency $[\Omega_{21}+(\Delta-\gamma)]-(2\Delta+\delta)$ disappears and is replaced by an oscillation at frequency $[\Omega_{21}+(\Delta-\gamma)]-\Delta$ leading to beats at frequency Δ. Note that even for small slit widths, no beats are predicted for orthogonal excitation.

The effect of a finite pulse width is of course greatest if the dephasing time is longer than the pulse width. In the case of orthogonal excitation, however, the effect is only seen in the rising flank of the signal. The conclusion is that for orthogonal excitation any dephasing time can be measured with confidence in the decaying flank, regardless of the pulse width, as long as the coherent time of the fields is short enough. In the case of parallel excitation, pulse width effects are present both in the rising flank as well as in the decaying flank, so a dephasing time can only be measured accurately if it is much shorter than the pulse.

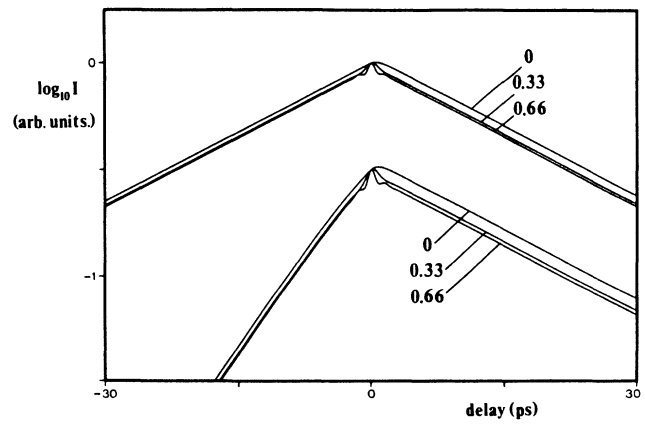

FIG. 8. The same parameters as in Fig. 7 except in the orthogonal polarization configuration, i.e., $\mathbf{E}_1\|\mathbf{E}_2$, $\mathbf{E}_3\|\mathbf{E}_4$, and $\mathbf{E}_1\perp\mathbf{E}_3$.

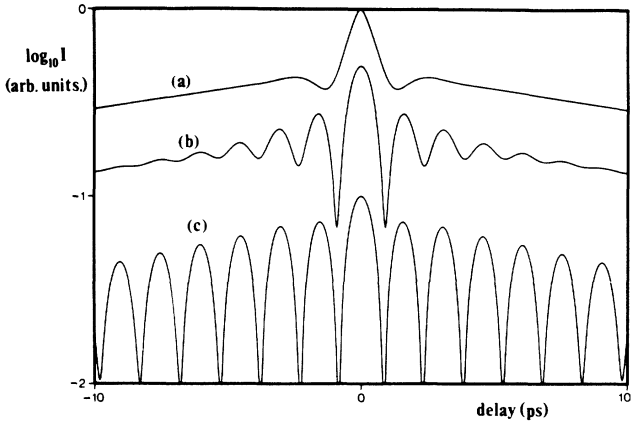

FIG. 9. Normalized RFD signal with parameter values $\Gamma_L=1.42$, $\gamma=0.05$, $\Delta=0.333$, and $\delta=0$ (all in ps^{-1}), cw fields, and parallel polarization configuration. The three traces show the signal for $\gamma_{slit}/(2\pi)=10.0$ (a), 0.5 (b), and 0.05 ps^{-1} (c).

The form of the incoherent CSRS signal is seen in Fig. 10, where the normalized signal with background subtracted is plotted as a function of the delay τ for various values of the coherence time of the Stokes field. Again two extreme cases, $\Gamma_S/\gamma \gg 1$ and $\Gamma_S/\gamma \ll 1$, can be discerned that have a similar impact on the form of the signal. The disappointing feature of incoherent CSRS is its prodigious coherence spike that becomes more and more dominant as the coherence time decreases, so a greater time resolution is offset by a deteriorating capacity to determine the vibrational coherence decay time.

Beats start to appear as the two-photon detuning is increased starting from $\Delta=0$ but the beats are confined to delays smaller than the coherence time. Furthermore, the tail of the signal still decays with 2γ [that is with $(T_2/2)^{-1}$] as long as the coherence time is relatively short. It has been checked numerically that effects of a smaller spectral response of the detector have a similar effect on these beats to that seen in the RFD signal. This conforms to the predictions made in Ref. 48.

The signal of incoherent TSRG is found to be always asymmetric (see Fig. 11) with the slow flank decaying with $\gamma=(T_2)^{-1}$ just as in RFD. This asymmetry should come as no surprise since it is in fact one of the assumptions made in the calculation. The assumption that the excitation pulse pair propagates along another path than the probe-pulse pair breaks the symmetry between these two pulse pairs, that is, their roles (i.e., excitation versus probing) are fixed and cannot be interchanged. The same could have been achieved by orthogonally polarizing the excitation pulse pair relative to the probe-pulse pair. The advantage of the asymmetry in TSRG is that the time resolution, proportional to $(\Gamma_P+\Gamma_L+\Gamma_S)^{-1}$, can easily be estimated from the experimental data. Note that the TSRG signal contains a coherence spike (at least for the parallel polarization considered here) due to the electronic contribution. It is evident from Eq. (31c) that this spike scales with the relative importance of the coherent and incoherent part of the fields. For completely coherent pulsed light the spike is absent whereas for completely incoherent cw light it dominates the signal.

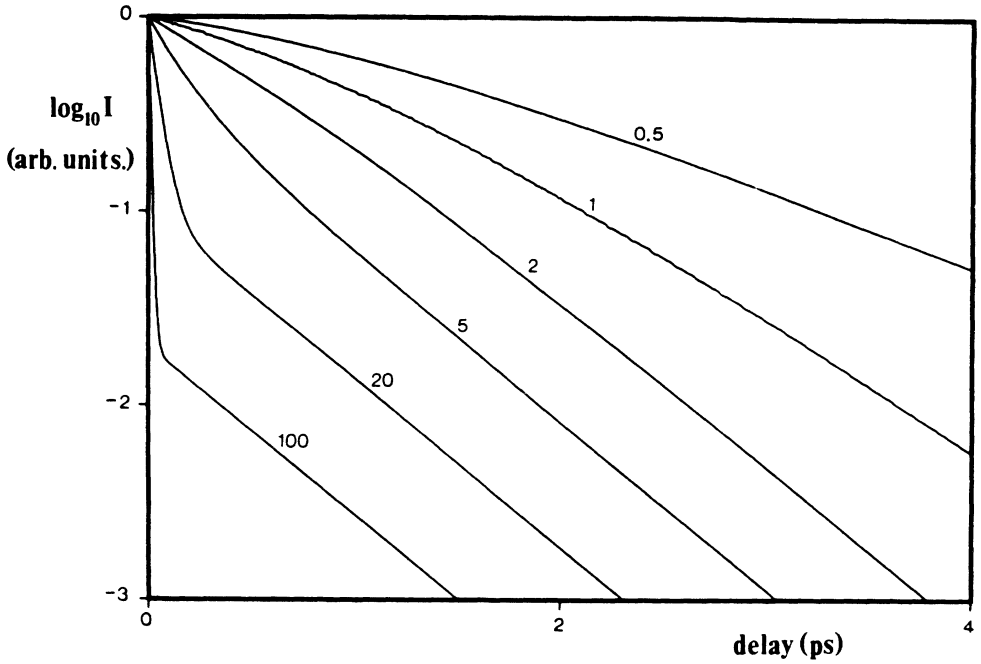

FIG. 10. Normalized incoherent CSRS signal intensity with background subtracted plotted as a function of the delay τ. The coherence rate Γ_S of the Stokes field varies from 0.5 to 100 ps^{-1} and $\gamma = 1$ ps^{-1}.

Again beats are observed if laser and Stokes are detuned as can be seen in Fig. 12. Unlike the beats in CSRS and RFD, the beats can be observed clearly even with broadband detection but it is found that the beats in TSRG are only visible at certain critical frequency detunings that depend on the field parameters in a complicated way.

The two fringe techniques (RFD, TSRG) have one obvious disadvantage: to monitor the fringes properly (and to avoid aliasing of Fourier components) huge amounts of data have to be sampled (for example a 500-cm^{-1} Raman transition leads to oscillations with a period of about 66 fs). This makes the use of high-repetition-rate pulse trains almost obligatory and prohibits the use of low-

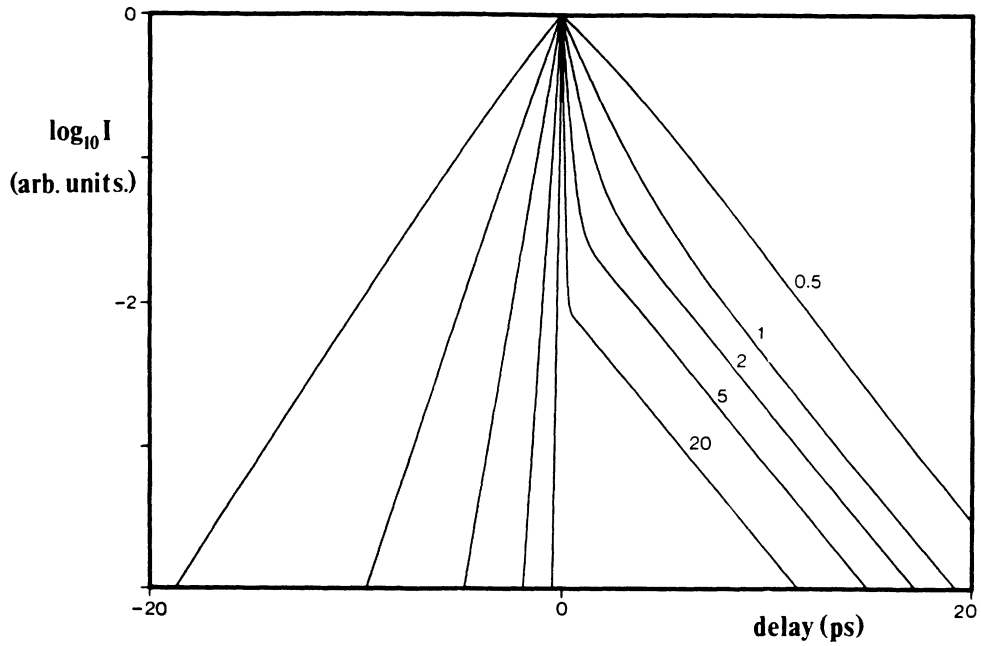

FIG. 11. Normalized incoherent TSRG signal intensity plotted as a function of delay. The parameters are chosen: $\Gamma_P = 0.1$, $\gamma = 0.4$, $\Delta = 0$, and $\Gamma_L + \Gamma_S$ varies from 0.5 to 20 (all in ps^{-1}).

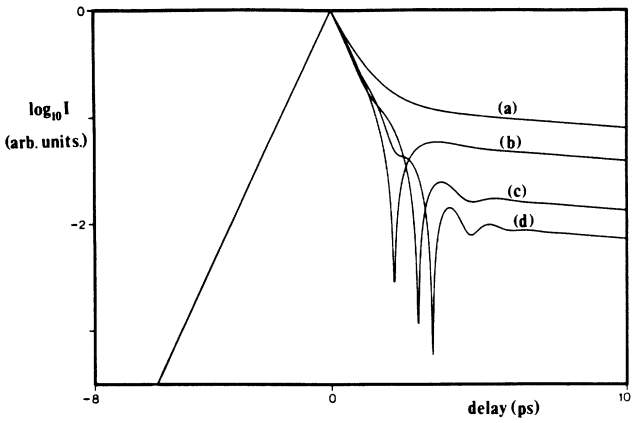

FIG. 12. The TSRG signal displays large dips for certain critical frequency detunings. Here $\Gamma_L+\Gamma_S=1.42$, $\Gamma_P=0.1$, $\gamma=0.05$, and $\Delta=0.0$ (a), 0.24 (b), 0.52 (c), and 0.74 (d) (all in ps^{-1}).

repetition-rate amplified pulses. One can imagine that the signal-to-noise ratio is dramatically improved if materials are studied that have an intermediate electronic resonance. However, if laser and Stokes pulses are both one-photon resonant, strong-field effects are to be expected, and the above theory becomes meaningless. In experiments with incoherent light in two-level systems (DFWM) it is found[29,49–51] that higher-order correlation functions of the fields become important, which leads to a degradation of the signal. As discussed in Ref. 52, the strong-field solution seems impossible to find analytically due to the fact that the total stochastic process contributed by all the pulses involved in pumping and probing is non-Markovian, and the coupling is strong. The same will evidently hold for strong-field stochastic Raman scattering.

III. OUTLINE OF THE RFD EXPERIMENT AND RESULTS

The layout of the experimental setup is shown in Fig. 13. Two Coherent CR-590 dye lasers (using rhodamine 6G dye) are synchronously pumped by a Coherent CR-10 mode-locked argon laser [pulse width $\cong$80 ps full width at half maximum (FWHM)] and produce pulses at a repetition frequency of 76 MHz. The dye lasers are tuned to the laser and Stokes frequencies (ω_L and ω_S, respectively), such that their difference frequency matches the Raman transition frequency of interest. One of the dye lasers operates with a three-plate birefringent filter while the other operates with a one-plate birefringent filter to yield incoherent pulses. Both dye lasers produce pulses with an autocorrelation of 10 ps (FWHM). The incoherent pulses additionally have a coherence spike of 700 fs (FWHM) which corresponds well with the observed laser spectrum.

The laser and Stokes beams are combined and split with a 50% beam splitter into an excitation and probe-pulse pair, each consisting of laser and Stokes pulses. The temporal overlap of the laser and Stokes pulses can be adjusted by a stepper motor (resolution 1 μm) and is

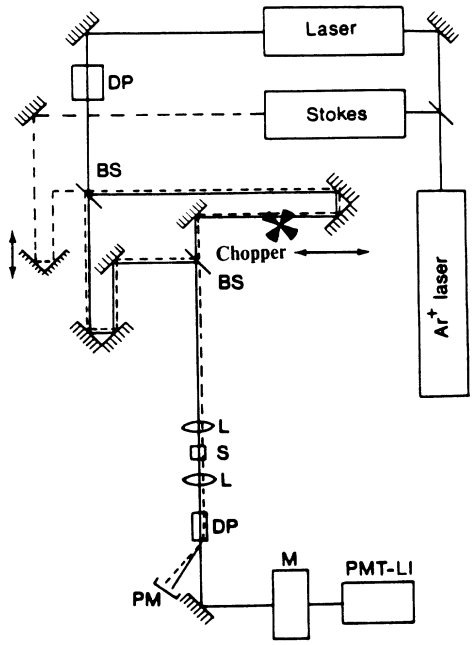

FIG. 13. Experimental setup for the measurement of the Raman-fringe decay. The following symbols are used: BS, beamsplitter; DP, direct-vision prism; *L*, lens; PM, power meter; *S*, sample; *M*, monochromator; PMT, photomultiplier tube; LI, lock-in amplifier.

optimized using cross correlation in a potassium dihydrogen phosphate (KDP) crystal. The probe-pulse pair is sent through an optical delay line with stepper motor (resolution 0.1 μm) before being made collinear—to within 0.8 mrad—with the excitation pulse pair. In the case of orthogonal excitation, the polarization of the excitation pulse pair is rotated over 90° using a set of mirrors, before being made collinear with the probe-pulse pair in a polarizing prism. Note that great care has been taken to avoid glass components in the setup. A corner cube, for example, can seriously affect the coherence and polarization properties of the fields. The beams are focused into the sample with a 5-cm achromatic lens and the signal (at the anti-Stokes frequency) is passed through a direct-vision prism and a grating monochromator before being detected with a photomultiplier. The signal intensity is then recorded as a function of the delay time between excitation and probe. The data obtained show oscillations—"Raman fringes"—associated with the vibrational transition frequency. To obtain the characteristic relaxation time, the amplitude of these fringes is plotted versus delay time.

In the experiments the excitation beam is modulated at 800 Hz with a mechanical chopper and the signal is lock-in amplified and digitized. To avoid overloading in case of parallel excitation the spontaneous emission from the dye lasers is suppressed with a direct-vision prism (after the laser dye laser) and a low-pass colored glass filter (RG600; after the Stokes dye laser). Furthermore, a piezoelectric mounted mirror applying a fast (4-kHz) phase modulation on the probe beam was necessary to average out interference effects. In case of orthogonal ex-

citation, a low-pass sharp cutoff filter (OG590) in the probe beam suffices to reduce the load and interference is absent.

The experiments were performed at the 524-cm^{-1} mode of methyl iodide and the 656-cm^{-1} mode of carbon disulfide, at room temperature (293±1.5 K). These two liquids provide two opposite regimes: $\Gamma_P \ll \gamma$ for CH_3I and $\Gamma_P \gg \gamma$ for CS_2. The samples of methyl iodide and carbon disulfide (both Merck, spectroscopic grade) were used without further purification. (Methyl iodide is photochemically unstable and was therefore refreshed before each run.)

To enable a discussion of the results and a comparison with theory, orthogonal and parallel excitation will be treated separately first in the broadband detection limit. These two different experimental results will be seen to yield significantly different results. Then the attention is focused on the influence of limited detection bandwidth, which again yields different results.

A. Orthogonal excitation and broadband detection

Typical results for this type of measurement for both CS_2 and CH_3I are presented in Fig. 14. The smooth curves are a least-squares fit of the data to the complete analytical expression including finite pulse width derived from theory. The main characteristics of the data obtained with this configuration are the following: (1) the fringe amplitude decays with a characteristic time equal to the vibrational dephasing time (T_2). The dephasing times of 21.3±0.1 ps for carbon disulfide and 2.4±0.2 ps for methyl iodide are in good agreement with earlier published results;[23,53,54] (2) the time resolution is obviously not limited by the pulse width of ≅10 ps, but rather by the correlation time of the fields; (3) the signal is asymmetric with respect to τ due to the fact that excitation and probe-pulse pair are not interchangeable because of their different polarization directions; (4) the frequency of the fringes is equal to the transition frequency of the vibrational mode within the spectral resolution of the Fourier transform of the data. For all of these observations the excellent agreement between experiment and theory should be noted.

The above results were obtained for resonant excitation of the vibrational mode. In other experiments it was found that off-resonant excitation, with $\Delta \cong 15$ cm^{-1}, yielded equal results. This can be expected from theory since the signal-to-noise ratio in these experiments was not high enough to observe the very small detuning oscillations which are predicted.

B. Parallel excitation and broadband detection

In Fig. 15(b) a typical result for this type of experiment is shown for CH_3I. The signal is now symmetric with respect to τ, due to the interchangeability of excitation and probe-pulse pair. Again it is found that the time resolution is not determined by the pulse width, but by the correlation time. A different type of result is found for CS_2 as is shown in Fig. 15(a). The signal is still symmetric, but no longer decays with the characteristic dephasing time. In fact, what is found is basically the result of the finite width of the pulses. This is confirmed nicely by theory.

In contrast to what was found for orthogonal excitation, a dramatic effect on the data is found for off-resonant excitation. Strong detuning oscillations are found for this case. It is found from the Fourier transform of the data that there are two oscillation frequencies: one at the usual vibrational transition frequency Ω_{21} and the other at the (detuned) laser difference frequency $\omega_L - \omega_S$.

C. Parallel excitation and monochromatic-noise excitation

The detuning oscillations observed for off-resonant excitation become much more pronounced when the detection bandwidth is set much smaller than the inverse relaxation time of the system. Figure 16 shows the results

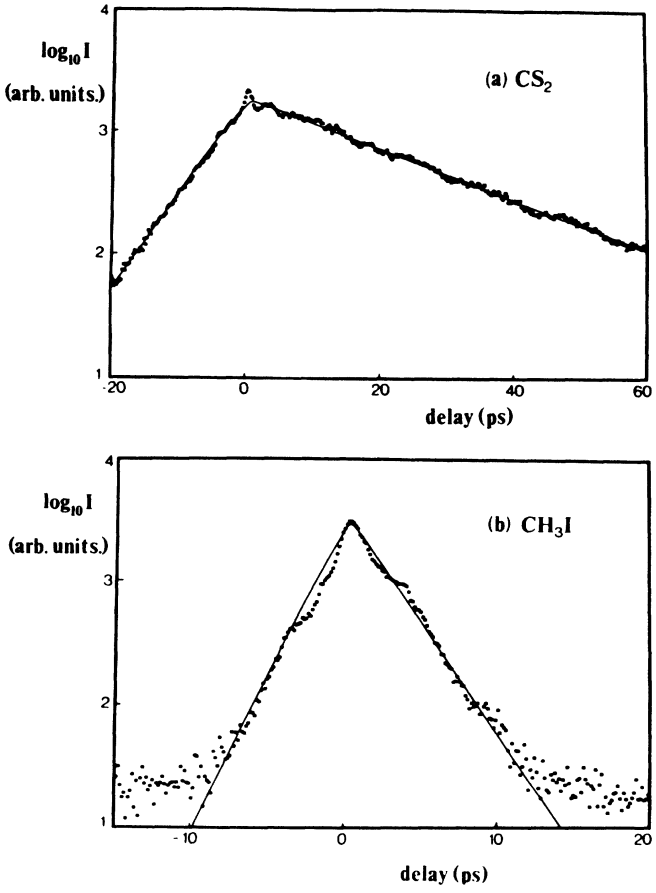

FIG. 14. Experimental data for orthogonal excitation in RFD experiments with broadband detection on carbon disulfide (a) and methyl iodide (b). The solid curve in (a) is a least-squares fit of the theoretical calculations (including the effect of a finite pulse width) to the data with $\Gamma_L = 4(2)$, $\Gamma_P = 0.141(1)$, $\gamma = 0.0469(2)$ (all in ps^{-1}). The data of (b) have not been fitted because of the significant departure from exponential decay for small τ. This feature is due to a malfunctioning of the analog-to-digital converter. The parameters used for the "handmade" fit are $\Gamma_L = 5$, $\Gamma_P = 0.19$, $\gamma = 0.42$ (all in ps^{-1}).

for experiments on CS_2 where the detuning from Raman resonance was set at 14.1 cm^{-1} and the signal is recorded as function of the delay time between excitation and probe for several detection frequencies. It is found that, although the detuning remains constant, the beat frequency changes with the detection frequency. For special settings of the detuning and the detection frequency even three different frequencies may be observed in the Fourier spectrum. In Fig. 17 the beat frequency is plotted as function of the detection frequency. The solid line shows the theoretical prediction. Note that the observed behavior is in good agreement with theory. Other predictions from theory, such as the observation of detuning oscillations with *resonant* excitation but with a detuned detection; and a $(2\delta+\Delta)$-beat frequency dependence for off-resonant excitation and monochromatic detection, smoothly changing to a Δ-beat frequency dependence in the broadband detection limit, are also confirmed nicely by theory.

Finally a word of comment on the relative merits of RFD compared to other incoherent techniques. First it should be noted that for orthogonal excitation this tech-

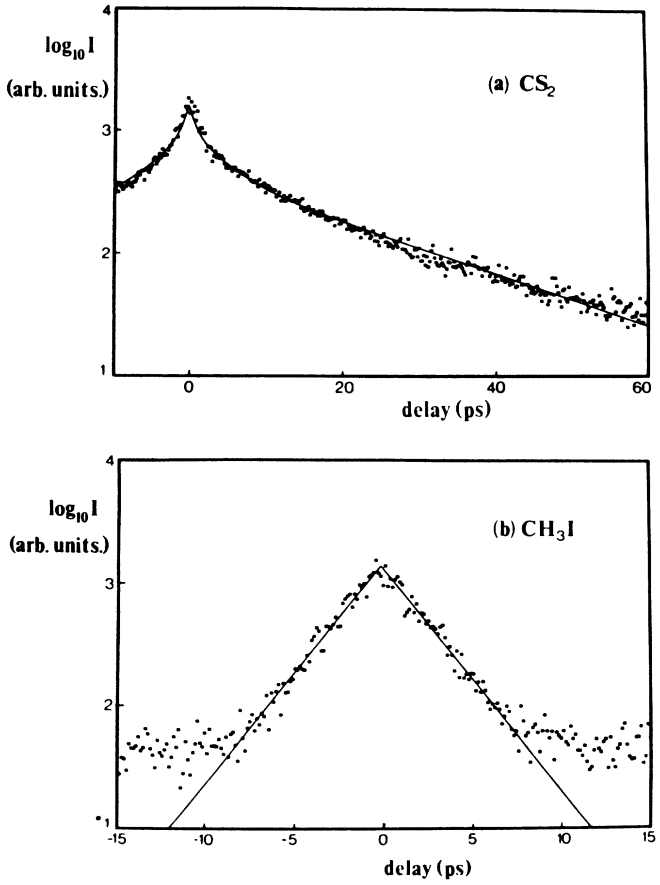

FIG. 15. Experimental data for parallel excitation in RFD experiments with broadband detection on carbon disulfide (a) and methyl iodide (b). The solid curve is a least-squares fit of the theoretical calculations to the data with (a) $\Gamma_L=1.2(2)$, $\Gamma_P=0.23(2)$, $\gamma=0.0487(7)$, and (b) $\Gamma_L=1.0(3)$, $\Gamma_P=0.09(5)$, $\gamma=0.39(5)$ (all in ps^{-1}).

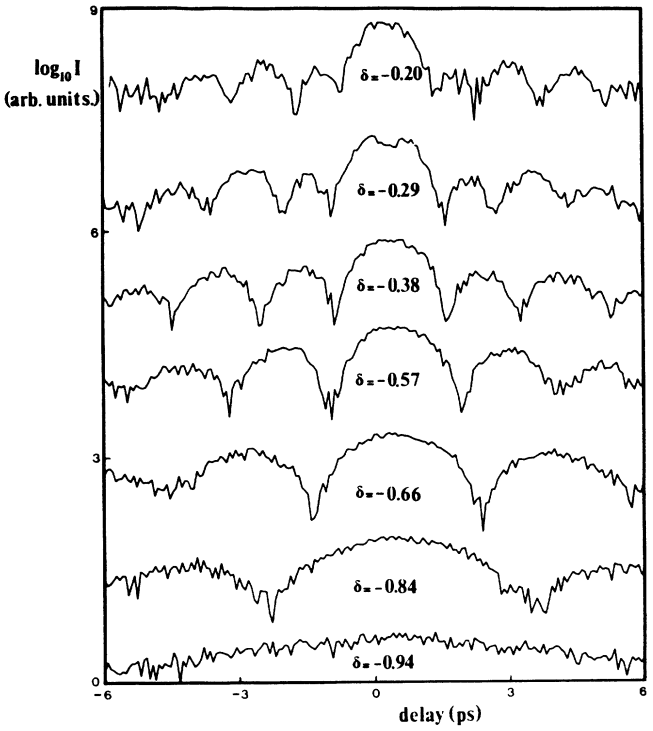

FIG. 16. Experimental data for parallel excitation in RFD experiments on carbon disulfide with pseudomonochromatic detection (detection bandwidth is 0.04 ps^{-1} FWHM) for different values of the detection detuning δ (in ps^{-1}). The Raman detuning Δ was set at 0.42 ps^{-1}.

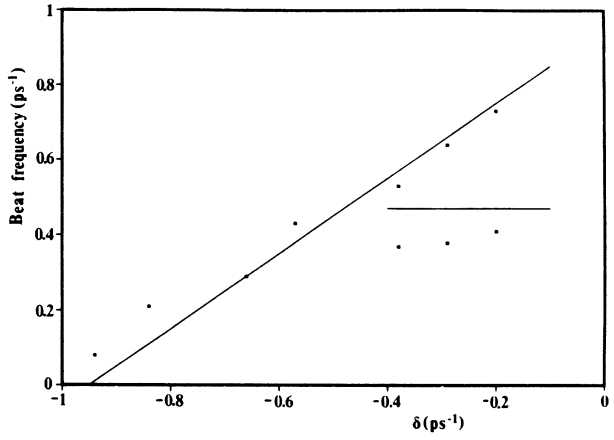

FIG. 17. The experimental beat frequencies taken from the Fourier transform of the same experimental data as used in Fig. 16, plotted vs the detection detuning δ. Note that the Fourier spectrum shows three peaks for $\delta > -0.4$ ps^{-1}. The solid line is the theoretical curve: $2\Delta+\delta$, with $\Delta=0.475$ ps^{-1}. The deviation from quantitative agreement between theory and experiment is largely due to the rather large uncertainty in the experimental value of Δ and the limited spectral resolution in the Fourier transform of the data.

nique yields a characteristic decay time equal to the dephasing time (T_2) which is independent of the pulse width. The signal has no background and also no "spike" is found on top of the signal which may make interpretation of the data ambiguous. Both these properties of the RFD experiments compare favorably to incoherent CSRS or CARS, which are only effective in the regime of $\gamma_{21}^{-1} < \Gamma_P^{-1}$, show a characteristic decay time of $T_2/2$, have a large background signal, and which do show a "spike." On the other hand, the RFD technique is quite similar to TSRG. The latter technique has one disadvantage in that it relies on an expensive apparatus to extract the signal from an enormous background. Furthermore, TSRG shows a spike around zero delay which dominates the signal for cw incoherent fields. So it may be concluded that the RFD technique is quite a powerful incoherent technique for measuring ultrafast dephasing times as long as the coherent beating effects can be avoided.

For all Raman processes described above it holds that the relaxation observed is equally affected by homogeneous as well as inhomogeneous dephasing of the vibrational transition. It has been suggested by many authors[22,25] that only a Raman echo[56] can discern between these two types of dephasing. It may be clear that since the Raman echo is in many cases unobservable even with low-repetition-rate high-power-amplified pulses,[57] a Raman echo using one of the interference techniques is out of the question.

ACKNOWLEDGMENTS

This research was partially supported by Stichting Scheikundig Onderzoek Nederland (SON) and Stichting Nederlands Wetenschappelijk Onderzoek (NWO).

[1]Some advances towards tunable femtosecond dye lasers are being made; see, e.g., K. Kurokawa, H. Kubota, and M. Nakazawa, Opt. Commun. **73**, 319 (1989).
[2]N. Morita and T. Yajima, Phys. Rev. A **30**, 2525 (1984).
[3]N. Morita, T. Yajima, and Y. Ishida, *Ultra-Fast Phenomena IV* (Springer, Berlin, 1986).
[4]T. Yajima and N. Morita, in *Methods of Laser Spectroscopy*, edited by Y. Prior *et al.* (Plenum, New York, 1986).
[5]M. Tomita and M. Matsuoka, J. Opt. Soc. Am. B **3**, 560 (1986).
[6]N. Morita, T. Tokizaki, and T. Yajima, J. Opt. Soc. Am. B **4**, 1269 (1987).
[7]R. Beach and S. R. Hartmann, Phys. Rev. Lett. **53**, 663 (1984).
[8]J. E. Golub and T. W. Mossberg, J. Opt. Soc. Am. B **3**, 554 (1986).
[9]H. Nakatsuka, M. Tomita, M. Fujiwara, and S. Asaka, Opt. Commun. **52**, 150 (1984).
[10]T. Hattori and T. Kobayashi, Chem. Phys. Lett. **133**, 230 (1987).
[11]M. Defour, J. C. Keller, and J. L. Le Gouet, J. Opt. Soc. Am. B **3**, 544 (1986).
[12]M. Fujiwara, R. Kuroda, and H. Nakatsuka, J. Opt. Soc. Am. B **2**, 1634 (1985).
[13]S. Asaka, H. Nakatsuka, M. Fujiwara, and M. Matsuoka, Phys. Rev. A **29**, 2286 (1984).
[14]H. Nakatsuka, Y. Matsumoto, K. Inouye, and R. Yano, Opt. Lett. **14**, 633 (1989).
[15]S. Saikan, T. Nakabayashi, Y. Kanematsu, and N. Tato, Phys. Rev. B **38**, 7777 (1988).
[16]S. Saikan, H. Miyamoto, Y. Tosaki, and A. Fujiwara, Phys. Rev. B **36**, 5074 (1987).
[17]K. Kurokawa, T. Hattori, and T. Kobayashi, Phys. Rev. A **36**, 1298 (1987).
[18]T. Kobayashi, A. Terasaki, T. Hattori, and K. Kurokawa, Appl. Phys. B **47**, 107 (1988).
[19]T. Kobayashi, T. Hattori, A. Terasaki, and K. Kurokawa, Rev. Phys. Appl. **22**, 1773 (1987).
[20]K. Misawa, T. Hattori, and T. Kobayashi, Opt. Lett. **14**, 453 (1989).
[21]N. Morita, K. Torizuka, and T. Yajima, J. Opt. Soc. Am. B **3**, 548 (1986).
[22]T. Hattori, A. Terasaki, and T. Kobayashi, Phys. Rev. A **35**, 715 (1987).
[23]M. Van Exter and A. Lagendijk, Opt. Commun. **56**, 191 (1985).
[24]P. M. Felker and G. V. Hartland, Chem. Phys. Lett. **134**, 503 (1987).
[25]Y. R. Shen, *The Principles of Nonlinear Optics* (Wiley, New York, 1986).
[26]T. K. Yee and T. K. Gustafson, Phys. Rev. A **18**, 1597 (1978).
[27]K. Wynne, M. Müller, D. Brandt, and J. D. W. Van Voorst, Chem. Phys. **125**, 211 (1988).
[28]R. Loudon, *The Quantum Theory of Light*, 2nd ed. (Oxford University Press, Oxford, 1983).
[29]P. Tchenio, A. Debarre, J.-C. Keller, and J.-L. Le Gouet, Phys. Rev. A **38**, 5235 (1988).
[30]S. Mukamel and E. Hanamura, Phys. Rev. A **33**, 3970 (1986).
[31]J. W. Goodman, *Statistical Optics* (Wiley, New York, 1985).
[32]G. V. Hartland and P. M. Felker, J. Chem. Phys. **91**, 5527 (1987).
[33]T. C. Corcoran, L. L. Connell, G. V. Hartland, B. F. Henson, and P. M. Felker, Chem. Phys. Lett. **147**, 517 (1988).
[34]G. V. Hartland, B. F. Henson, and P. M. Felker, J. Chem. Phys. **91**, 1478 (1989).
[35]M. Van Exter and A. Lagendijk, Chem. Phys. Lett. **146**, 482 (1988).
[36]K. Wynne, M. Müller, and J. D. W. Van Voorst, Phys. Rev. Lett. **62**, 3031 (1989).
[37]M. Müller, K. Wynne, and J. D. W. Van Voorst (unpublished).
[38]B. S. Wherrett, A. L. Smirl, and T. F. Bogges, IEEE J. Quantum Electron. **QE-19**, 680 (1983).
[39]J. G. Fujimoto and T. K. Yee, IEEE J. Quantum Electron. **QE-22**, 1215 (1986).
[40]K. Wynne and M. Müller (unpublished).
[41]M. Schubert and B. Wilhelmi, *Nonlinear Optics and Quantum Electronics* (Wiley, New York, 1986).
[42]J. P. Heritage, Appl. Phys. Lett. **34**, 470 (1979).
[43]M. Van Exter, A. Lagendijk, and E. Spaans, Opt. Commun. **59**, 411 (1986).
[44]M. Van Exter and A. Lagendijk, Opt. Commun. **70**, 433 (1989).
[45]M. De Mazière, C. Sierens, and D. Schoemaker, J. Opt. Soc. Am. B **6**, 2376 (1989).
[46]M. D. Levenson and G. L. Eesley, Appl. Phys. **19**, 1 (1979).

[47]G. L. Eesley, M. D. Levenson, and W. M. Tolles, IEEE J. Quantum Electron. **QE-14**, 45 (1978).
[48]M. A. Dugan, J. S. Melinger, and A. C. Albrecht, Chem. Phys. Lett. **147**, 411 (1988).
[49]R. Beach, D. DeBeer, and S. R. Hartmann, Phys. Rev. A **32**, 3467 (1985).
[50]P. Tchenio, A. Debarre, J.-C. Keller, and J.-L. Le Gouet, J. Opt. Soc. Am. B **5**, 1293 (1988).
[51]M. Defour, J.-C. Keller, and J.-L. Le Gouet, Phys. Rev. A **36**, 5226 (1987).
[52]P. Tchenio, A. Debarre, J.-C. Keller, and J.-L. Le Gouet, Phys. Rev. Lett. **62**, 415 (1989).
[53]R. B. Wright, M. Schwartz, and C. H. Wang, J. Chem. Phys. **58**, 5125 (1973).
[54]N. Kohles and A. Laubereau, Chem. Phys. Lett. **138**, 365 (1987).
[55]R. F. Loring and S. Mukamel, J. Chem. Phys. **83**, 2116 (1985).
[56]S. R. Hartmann, IEEE J. Quantum Electron. **QE-4**, 802 (1968).
[57]M. Müller, K. Wynne, and J. D. W. Van Voorst, Chem. Phys. **128**, 549 (1988).